Neuron, Vol. 38, 805–817, June 5, 2003, Copyright ©2003 by Cell Press

A Novel Network of Multipolar Bursting Interneurons Generates Theta Frequency Oscillations in Neocortex

Maria Blatow,[1,4] Andrei Rozov,[1,2,4] Istvan Katona,[1,5] Sheriar G. Hormuzdi,[1] Axel H. Meyer,[1] Miles A. Whittington,[3] Antonio Caputi,[1] and Hannah Monyer[1,*]

[1]Department of Clinical Neurobiology
University Hospital for Neurology
Im Neuenheimer Feld 364
69120 Heidelberg
Germany

[2]Department of Experimental Neurophysiology
Faculty of Earth and Life Science
Vrije University Amsterdam
De Boelelaan 1087
1081 HV Amsterdam
The Netherlands

[3]School of Biomedical Sciences
University of Leeds
Leeds LS2 9NL
United Kingdom

Summary

GABAergic interneurons can phase the output of principal cells, giving rise to oscillatory activity in different frequency bands. Here we describe a new subtype of GABAergic interneuron, the multipolar bursting (MB) cell in the mouse neocortex. MB cells are parvalbumin positive but differ from fast-spiking multipolar (FS) cells in their morphological, neurochemical, and physiological properties. MB cells are reciprocally connected with layer 2/3 pyramidal cells and are coupled with each other by chemical and electrical synapses. MB cells innervate FS cells but not vice versa. MB to MB cell as well as MB to pyramidal cell synapses exhibit paired-pulse facilitation. Carbachol selectively induced synchronized theta frequency oscillations in MB cells. Synchrony required both gap junction coupling and GABAergic chemical transmission, but not excitatory glutamatergic input. Hence, MB cells form a distinct inhibitory network, which upon cholinergic drive can generate rhythmic and synchronous theta frequency activity, providing temporal coordination of pyramidal cell output.

Introduction

There is an increasing body of evidence indicating that, in addition to providing the main source of inhibition in the brain, GABAergic interneurons play a pivotal role in synchronous and oscillatory network activity (Buzsaki and Chrobak, 1995; McBain and Fisahn, 2001; Somogyi et al., 1998). GABAergic interneurons can phase the output of pyramidal cells, giving rise to oscillatory activity in different frequency bands (Cobb et al., 1995; Tamas et al., 2000; Whittington et al., 1995; Ylinen et al., 1995a, 1995b). Furthermore, recent studies indicated that gap junction coupling of interneurons provides a powerful mechanism that aids in synchronizing network activity. Since gap junction coupling occurs preferentially between interneurons of the same type, it may delineate highly specialized inhibitory networks (Beierlein et al., 2000; Galarreta and Hestrin, 1999; Gibson et al., 1999; McBain and Fisahn, 2001; Tamas et al., 2000; Venance et al., 2000).

To better understand the precise role of a specific interneuron population in the functional architecture of the cortex, detailed morphological and physiological information about the synaptic and input/output properties of the given cell type are required. The parvalbumin (PV) containing FS cells provide a good example of how an interneuron population can be studied with respect to morphology, intrinsic firing, and network properties (Du et al., 1996; Freund and Buzsaki, 1996; Geiger et al., 1997; Martina et al., 1998; Traub et al., 1999). However, the identification of GABAergic interneurons in the acute slice preparation is often a difficult enterprise, particularly if such studies are carried out in brain regions other than the hippocampus.

To make subsets of GABAergic interneurons easily accessible for further detailed functional analysis, we have generated transgenic mice in which distinct GABAergic interneuron subclasses selectively express the in vivo marker EGFP (Caputi et al., 2000; Meyer et al., 2002). In the present study, in mice expressing EGFP under the control of the PV promoter, we identified a previously undescribed cell type, which, based on morphology and firing pattern, we named multipolar bursting (MB) cells.

These interneurons constitute a subset of PV-positive neurons in layer 2/3 of the frontal and somatosensory cortex that differs from the majority of PV-positive neurons, the FS cells (Kawaguchi, 1995), in various morphological and functional properties. MB cells are coupled by chemical and electrical synapses and constitute an inhibitory network that is well suited for the generation of rhythmic activity in the upper layers of the cortex. Carbachol-induced theta frequency oscillations (4–7 Hz) in MB cells can drive synchronized inhibition of pyramidal cells. Synchrony does not depend on excitatory chemical transmission, since it was insensitive to the application of the AMPA receptor (AMPAR) channel blocker NBQX. However, synchrony requires both GABAergic chemical transmission and electrical coupling, since it was disrupted by the application of the $GABA_A$ channel blockers SR-95531 and bicuculline and was absent in connexin 36 (Cx36) knockout mice.

Results

Multipolar Bursting Cells Constitute a Novel and Distinct Interneuron Type

Initially, finding MB cells in the slice was aided by the expression of EGFP in transgenic mice expressing this

*Correspondence: monyer@urz.uni-hd.de
[4]These authors contributed equally to this work.
[5]Present address: Institute of Experimental Medicine, Hungarian Academy of Science, H-1450 Budapest P.O.B. 67, Hungary.

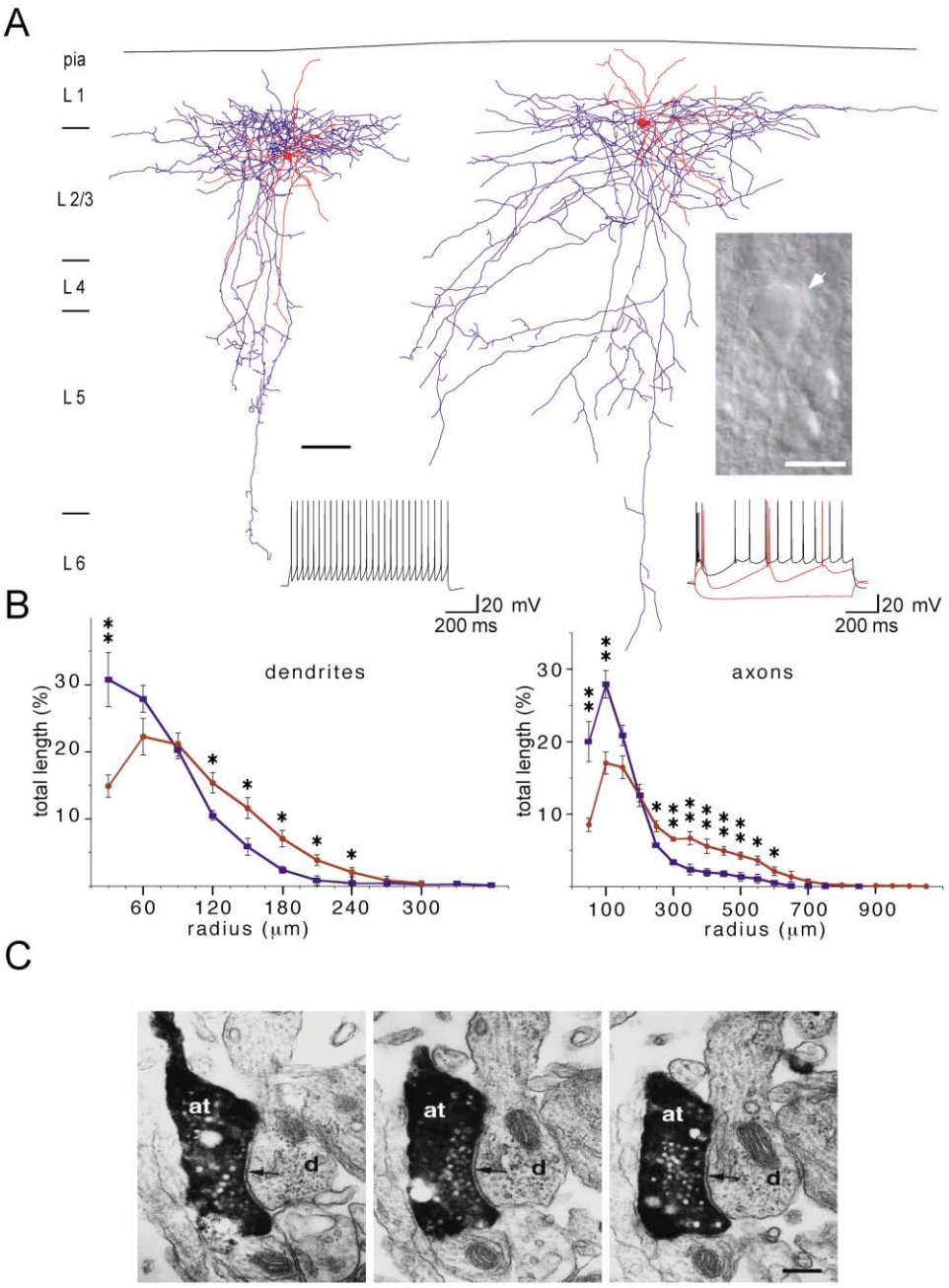

Figure 1. Morphological and Functional Identification of MB Cells

(A) Right panels relate to MB cells, left panels to FS cells. Representative reconstructions of the dendritic (red) and axonal (blue) arbors of biocytin-filled interneurons (scale bar is 100 μm) and typical firing patterns of APs upon depolarizing/hyperpolarizing current injection. The resting membrane potentials were −62 mV and −70 mV for the MB cell and the FS cell, respectively. The IR-DIC picture shows the typical appearance of a MB cell (indicated by arrow) in the slice (scale bar is 20 μm).

(B) Sholl plots of dendritic (left) and axonal (right) extensions expressed in percent of total dendrite or axon length and plotted versus the distance from the soma. MB cells are depicted in red and FS cells in blue. Error bars are given as SEM (*$p < 0.05$; **$p < 0.01$).

(C) MB cells innervate dendrites. Serial ultrathin sections reveal that the axon terminal (at) of a biocytin-filled MB cell forms a symmetrical (presumably GABAergic) synapse (indicated by arrow) on the dendritic shaft (depicted by "d") of its postsynaptic partner, which is presumably a pyramidal cell. This synaptic contact was found in layer 2/3 of the frontal cortex. Scale bar is 0.2 μm.

in vivo marker under the control of the PV promoter. Once familiar with their location and cell shape, however, we also found them easily in slices obtained from wild-type mice. MB cells can be readily recognized in slices from wild-type mice by their location close to the border between layers 1 and 2 and their appearance in the infrared differential interference contrast (IR-DIC) video image (Figure 1A). These neurons have large round

Table 1. Comparison of Basic Electrophysiological Properties of MB Cells and FS Cells

Cell Type	Input Resistance (MΩ)	AP Amplitude (mV)	AP Half Width (ms)	Main Firing Frequency (Hz)	Burst Frequency (Hz)	AHP Amplitude (mV)	AHP Duration (ms)	Vm (mV)	Threshold Potential
MB	111 ± 39	80.6 ± 9	0.9 ± 0.3	12.8 ± 2,3**	70.8 ± 19.8	9.2 ± 5.2	166 ± 37	−60 ± 3**	−43 ± 2.7*
FS	82 ± 31	77 ± 6	0.7 ± 0.1	38 ± 9**	–	–	–	−73 ± 3**	−37 ± 3*

Main firing frequency, resting membrane potential (Vm), and threshold potential were significantly different in MB cells and FS cells (**$p < 0.0001$; *$p < 0.001$, $n = 11$ for each measurement). AHP: afterhyperpolarization. Firing properties were analyzed upon the same current injection for both cell types. Stimulus intensity was 500 pA and was sufficient to drive regular firing of FS cells during the entire time of current injection (1 s).

or oval cell bodies (19 ± 4 μm, n = 12) and one or several visible thick dendrites. The typical resting membrane potential of MB cells is around −60 mV, which is significantly higher than that of FS cells (−73 mV; Table 1). Their action potential (AP) firing pattern upon prolonged depolarizing current injection is characterized by an initial burst of two or three APs followed by a pronounced afterhyperpolarizing gap and a subsequent train of regular spiking, low-frequency APs (Figure 1A, right trace). The firing pattern of MB cells is different from that exhibited by typical FS PV-positive interneurons (Figure 1A, left trace; Kawaguchi, 1995; Reyes et al., 1998). The firing frequency in the regular spiking part (main firing frequency) was significantly lower than the firing rate of FS cells (Table 1), whereas input resistance and spike half width did not differ between the two cell types. These and other basic electrophysiological properties are summarized in Table 1.

For morphological analysis, MB cells (n = 12) and FS cells (n = 8) were filled with biocytin. Both MB cells and FS cells appeared as multipolar neurons, however, with significantly different numbers of primary dendrites (4.4 ± 1.3 for MB cells, 6.75 ± 0.5 for FS cells, $p < 0.05$). For detailed analysis of their dendritic and axonal arbors, MB cells (n = 8; Figure 1A, right cell) and FS cells (n = 5; Figure 1A, left cell) were reconstructed and Sholl analysis was performed. Figure 1B shows the percentage of the total dendritic (left plot) and axonal (right plot) length plotted versus the distance from the cell body. In MB cells and FS cells, 85% of the dendrites were located in a distance of 150 ± 20 μm and 120 ± 10 μm from the soma, respectively, and MB cell dendrites were branching more distally than those of FS cells. Of note is the difference of the axonal arborization pattern of MB cells compared to FS cells. MB cells have a wider axonal spread than FS cells (see also Figure 1A). The main fraction of the axonal arbor in MB cells (85%) was located within a radius of 420 ± 60 μm around the cell body with considerable extensions into layer 4, whereas 85% of the FS cell axons were restricted within an area of 210 ± 50 μm around the cell body, thus projecting mainly in the region of the dendritic tree ($p < 0.001$).

Next, the efferent connectivity pattern of MB cells was investigated, since it gives insight into the function of specific cells within a neuronal network. To this end, an analysis of the postsynaptic target distribution of biocytin-filled MB cells (n = 3) at the electron microscopic level was performed. We restricted our analysis to layer 2/3, since reconstructions of biocytin-filled neurons had shown that the vast majority of putative axon terminals of MB cells are located in these layers (Figure 1A). All biocytin-filled axon terminals formed symmetrical synapses, a characteristic of cortical GABAergic neurons. Biocytin-filled axon terminals were selected randomly in the electron microscope and 95 of them were followed through serial electron microscopic sections and analyzed in detail at the ultrastructural level. The majority of terminals targeted dendritic shafts (70 out of 95, 73.7%; Figure 1C). In addition, some of the labeled boutons formed synapses on the neck or head of dendritic spines (17 out of 95, 17.9%). Occasionally synapses were also found perisomatically, e.g., on cell bodies and proximal dendrites (8 out of 95, 8.4%). In this latter case, the nuclei of the target cells were not invaginated, suggesting that these postsynaptic neurons were principal cells. Taken together, the postsynaptic target analysis showed that MB cells target mainly the dendritic domain of postsynaptic cells and belong to the family of cortical dendritic inhibitory neurons (Somogyi et al., 1998), in contrast to FS cells, which have been shown to be perisomatic inhibitory neurons (Kawaguchi and Kubota, 1997).

Neurochemical content is a frequent criterion used to classify and characterize the heterogeneous group of GABAergic interneurons (Freund and Buzsaki, 1996). Since EGFP was expressed under the control of the PV promoter in transgenic mice, we expected MB cells to be PV positive. Although the correct expression of the transgene had been previously verified in the neocortex (Meyer et al., 2002), we wanted to exclude misexpression in MB cells. The presence of PV in MB cells was confirmed by immunolabeling of biocytin-filled cells (10 of 10 cells). Since a subpopulation of bitufted interneurons with a similar firing pattern has been reported to express calretinin (CR) and vasoactive intestinal peptide (VIP; Cauli et al., 2000; Rozov et al., 2001), we also tested for the presence of these markers in MB cells. None of the analyzed cells were positive for VIP (n = 9), and 4 out of 11 cells showed weak CR immunoreactivity. In contrast, 9 out of 9 MB cells were calbindin-D28k (CB) positive (Figure 2A). To exclude the possibility of filter transparence, pyramidal cells (n = 4) and FS cells (n = 3) were filled with biocytin, and subsequently stainings for PV and CB were performed. No signal was detected in pyramidal cells and only PV, but not CB, immunoreactivity was found in FS cells (data not shown).

Colocalization of PV and CB in the neocortex has been reported in rats and the percentage of double-positive cells decreased during development (Alcantara et al., 1996; van Brederode et al., 1991). To examine whether colocalization of PV and CB persisted in MB cells in adult mice, we performed immunolabeling of biocytin-

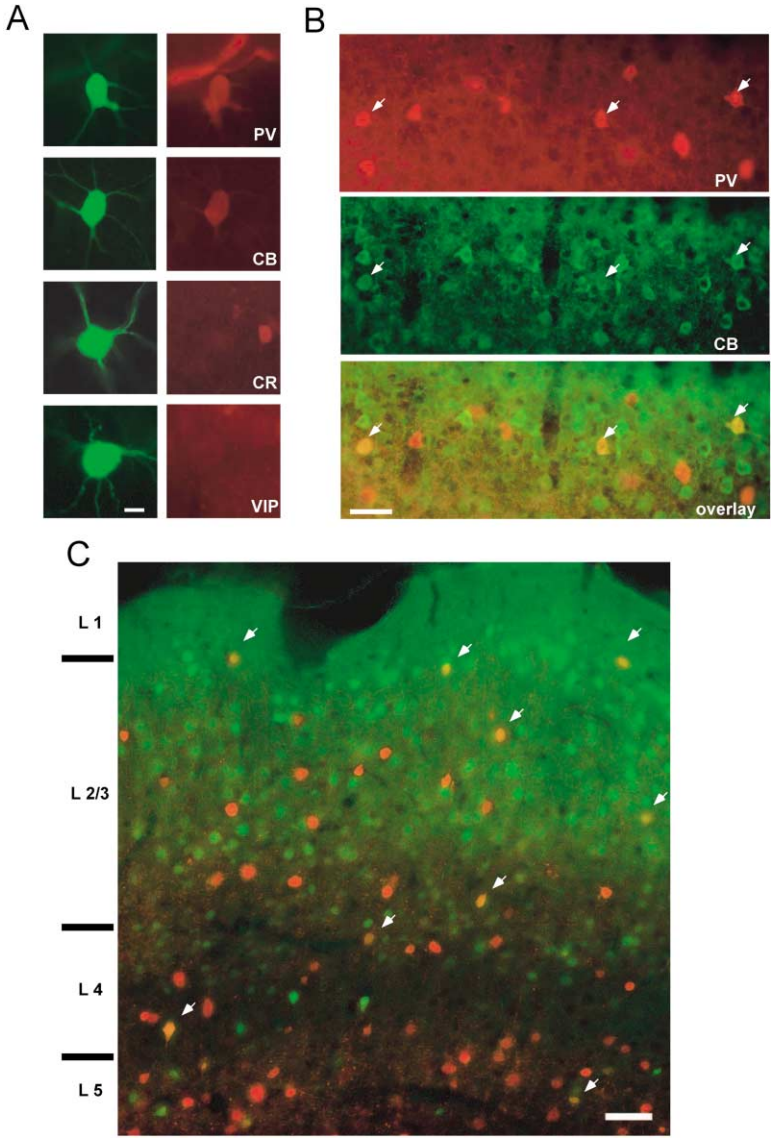

Figure 2. Immunocytochemical Signature of MB Cells

(A) Biocytin-filled MB cells (green, left four panels) stained with antibodies against the neurochemical markers (red, right four panels) parvalbumin (PV), calbindin-D28k (CB), calretinin (CR), and vasoactive intestinal peptide (VIP). Scale bar (10 μm) applies for all images.

(B) Double immunostaining for parvalbumin (red, upper panel) and calbindin-D28k (green, middle panel) in layer 2/3 of mouse frontal cortex. Lower panel shows the overlay. Arrows indicate double positive cells. Scale bar is 50 μm.

(C) Distribution of double positive cells across different cortical layers. Double immunostaining for PV (red) and CB (green) shown as an overlay. Arrows indicate double positive cells (yellow). Scale bar is 100 μm.

filled cells in P (postnatal) 28-day-old mice, where we continued to see expression of PV (4 of 5 cells) and CB (5 of 5 cells, data not shown). To estimate the percentage of double-positive cells within the PV-positive cell population in layer 2/3 of the frontal and somatosensory cortex, we performed double-immunofluorescence staining for PV and CB (Figures 2B and 2C). Nine microscopic fields (1 × 5 mm) were analyzed in P14 (3 mice) and eighteen in P28 (3 mice) animals. The analysis revealed that 32.8% ± 8% of PV-positive cells in cortical layer 2/3 of P14 mice also expressed CB. The density of PV-positive cells and the percentage of coexpression (35.3% ± 6%) were not changed in P28 animals. Figure 2B shows double positive cells in layer 2/3 of mouse frontal cortex. Although all experiments in this study were done in layer 2/3, it is possible that MB cells also exist in other cortical layers, since we observed double positive cells also in layers 4 and 5 (Figure 2C). Whether all double positive neurons are MB cells or whether some of them belong to yet another cell population expressing both markers cannot be determined.

Taken together, our data confirmed that MB cells constitute a distinct interneuron population different from the previously described PV-positive FS cells.

Synaptic Connectivity and Plasticity of MB Cells

Clearly one interesting and important question studying a novel neuronal subtype concerns the synaptic targets and the forms of synaptic plasticity at the different synapses. Simultaneous whole-cell recordings were made from pairs of synaptically connected MB cells and layer 2/3 pyramidal cells. MB cells innervated pyramidal cells quite commonly (success rate 41%), and the pattern of inhibitory postsynaptic potentials (IPSPs) exhibited on average paired-pulse facilitation (PPF) at a 100 ms interpulse interval. The average amplitude of the first IPSP was 1.21 ± 1.18 mV, and the average paired-pulse ratio (PPR) calculated as the ratio of IPSP2/IPSP1 was 1.27 ± 0.6 (Figure 3A, n = 41). Application of bicuculline (10 μM) completely blocked postsynaptic responses in pyramidal cells, confirming the GABAergic nature of the connection (n = 5, data not shown). MB cells received

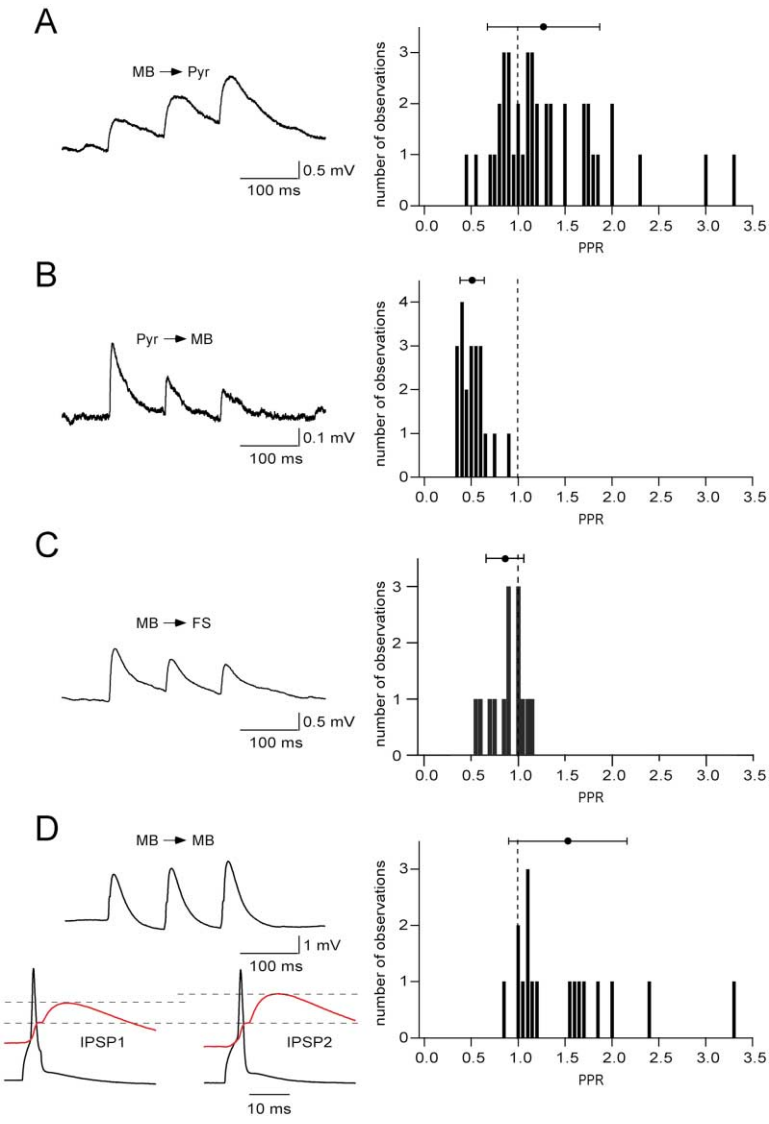

Figure 3. Short-Term Synaptic Plasticity in Different Circuits Formed by MB Cells

Simultaneous whole-cell recordings were made from synaptically connected neurons. Left panels show average traces of postsynaptic responses to a 10 Hz train of three APs. Histograms summarize data from a number of pairs and show the distribution of PPRs of postsynaptic potentials for the respective type of connection. Symbols above the histograms give the mean (± standard deviation) PPRs. Since high chloride (30 mM)-containing intracellular solution was used, IPSPs were depolarizing (chloride reverse potential was around −40 mV).

(A) Presynaptic, MB cell; postsynaptic, pyramidal cell (Pyr).

(B) Presynaptic, pyramidal cell; postsynaptic, MB cell.

(C) Presynaptic, MB cell; postsynaptic, FS cell.

(D) Presynaptic, MB cell; postsynaptic, MB cell. Expanded traces illustrate how IPSPs were dissected from gap junction-transmitted reflections of APs.

excitatory input from layer 2/3 pyramidal cells, characterized by strong paired-pulse depression of excitatory postsynaptic potentials (EPSPs). The average PPR was 0.51 ± 0.13, and the average EPSP1 amplitude was 0.38 ± 0.25 mV (Figure 3B, n = 21). Eleven of these pairs were reciprocal. However, the pyramidal cell to MB cell connectivity was substantially lower (success rate 18%), suggesting that the main excitatory input to MB cells derives from another cell population (see Discussion).

FS cells extensively innervate both principal neurons and interneurons in their proximity and are an important element for feedback inhibition (Gupta et al., 2000; Reyes et al., 1998). FS cells are connected to each other via both chemical and electrical synapses and have been proposed to form an inhibitory network participating in various oscillatory rhythms (Galarreta and Hestrin, 1999; Gibson et al., 1999; Penttonen et al., 1998; Traub et al., 1999; Tsodyks et al., 2000). To assess the interaction between MB cells and FS cells, we tested their connectivity. Although it was possible to find MB cell input to FS cells (Figure 3C, success rate 26%, average IPSP1 amplitude 0.77 ± 0.62 mV, average PPR 0.86 ± 0.2, n = 15), we could not find any connections in the opposite direction in 57 tested cell pairs. In addition, no gap junction coupling was observed between MB cells and FS cells. We conclude that MB cells are most likely not a target of FS cells and that these two types of interneurons belong to functionally distinct networks.

When two MB cells were found close to each other (40–200 μm; Figure 4D), they were almost always coupled via gap junctions (Figure 4A, n = 67, success rate 96%, coupling coefficient 0.08 ± 0.05) in addition to uni- or bidirectional chemical transmission. Despite the fact that in many pairs IPSPs were "contaminated" by large gap junction responses, in most cases where accurate measurements were possible, inhibitory connections between MB cells showed strong PPF (Figure 3D, average IPSP1 amplitude 1.06 ± 0.83 mV, average PPR 1.53 ± 0.63, n = 17). Exact measurements of IPSP amplitudes and PPR in MB cell to MB cell connections were possible, when the postsynaptic response was clearly

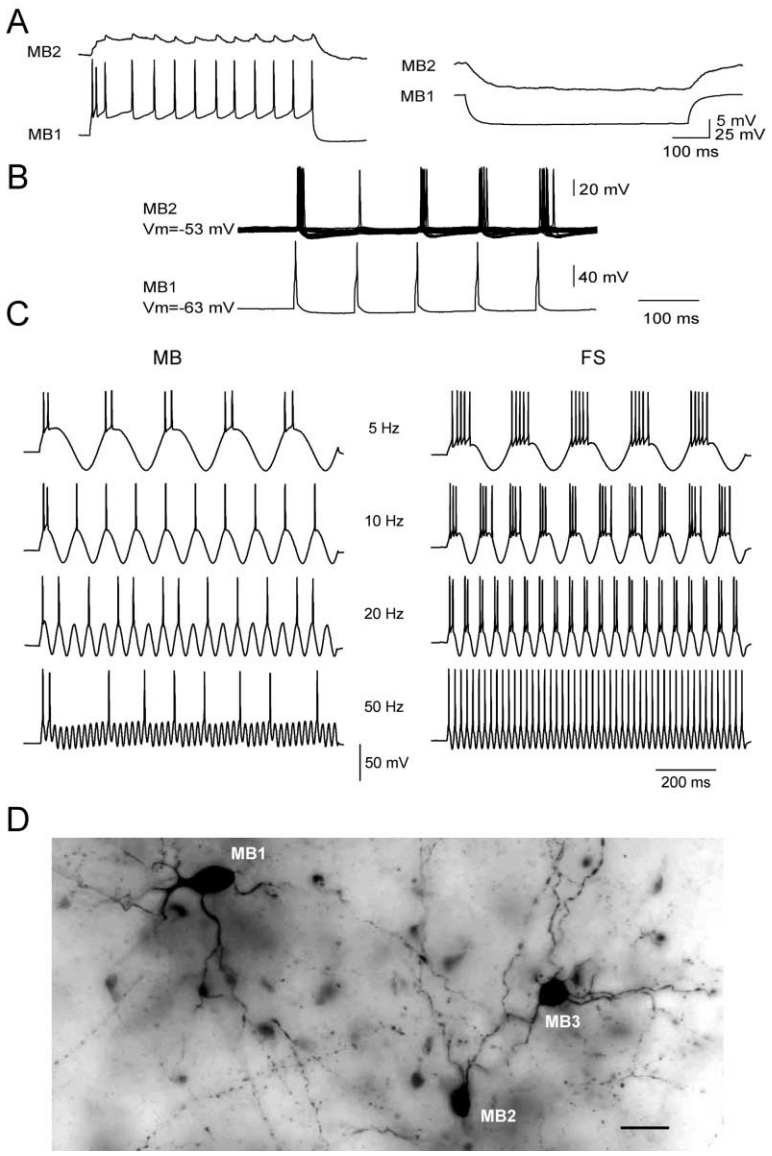

Figure 4. Electrical Coupling and Intrinsic Firing Properties Allow Synchronization of MB Cells at Low Frequencies

(A and B) Gap junction coupling between two MB cells.

(A) The voltage response of MB cell1 after depolarizing (left) and hyperpolarizing (right) current injection is also detectable in MB cell2.

(B) A 10 Hz train of APs evoked in MB cell1 was highly effective to elicit and synchronize APs in MB cell2, which was depolarized close to threshold. The upper trace is an overlay of 50 consecutive sweeps.

(C) Firing patterns of MB cells (left) and FS cells (right) in response to sinusoidal waveform current injections at different frequencies but same amplitudes. The amplitude of the current injection was minimal and sufficient for FS cells to follow at all tested frequencies. Note that MB cells were unable to reproduce high frequencies.

(D) Biocytin filling of three MB cells with gap junction coupling between MB cell1 and MB cell2 as well as between MB cell2 and MB cell3, illustrating a putative segment of the MB cell network. Scale bar is 20 μm.

biphasic, thus permitting the separation of the gap junction component from the IPSP component, with the first phase (gap junction component) starting at the time of the peak of the AP and the second phase (IPSP component) starting with a delay (Figure 3D, expanded traces). Altogether the results suggest that MB cells are a homogenous interneuron population. They are extensively coupled via chemical and electrical synapses and establish a distinct inhibitory network with output properties different from those of the FS interneuron network.

Carbachol-Induced Theta Frequency Oscillations in the MB Cell Network

MB cells may share excitation via gap junctions and fire synchronously, thereby providing coordinated inhibition of downstream neuronal populations. This hypothesis was tested in pairs of electrically coupled MB cells. Indeed, when cell 2 was depolarized close to threshold, a 10 Hz train of APs elicited in cell 1 was able to evoke APs in cell 2. The robust gap junction coupling was highly efficient in synchronizing pre- and postsynaptic activity, as shown in Figure 4B ($n = 3$). However, cell 2 fired at frequencies lower than 10 Hz. To compare the output characteristics of MB cells and FS cells in response to periodic changes in membrane potential, we injected sinusoidal waveform currents at 5, 10, 20, and 50 Hz to these interneurons. Since higher amplitude of injected current is required to trigger FS cell spiking (due to the significantly bigger difference between resting membrane and threshold potential in FS cells; Table 1), the amplitude of sinusoidal waveform currents was the same for both cell types and was selected to be minimal but sufficient for FS cells to follow at all tested frequencies. At 5 Hz, MB cells fired bursts of APs on top of each oscillation cycle and at 10 Hz only one AP, but at higher frequencies they were unable to follow the waveform current injection (Figure 4C, left traces, $n = 5$). In contrast, FS cells were readily firing APs on top of each oscillation cycle at 50 Hz (Figure 4C, right traces, $n = 5$). This suggests that MB cells output profiles may

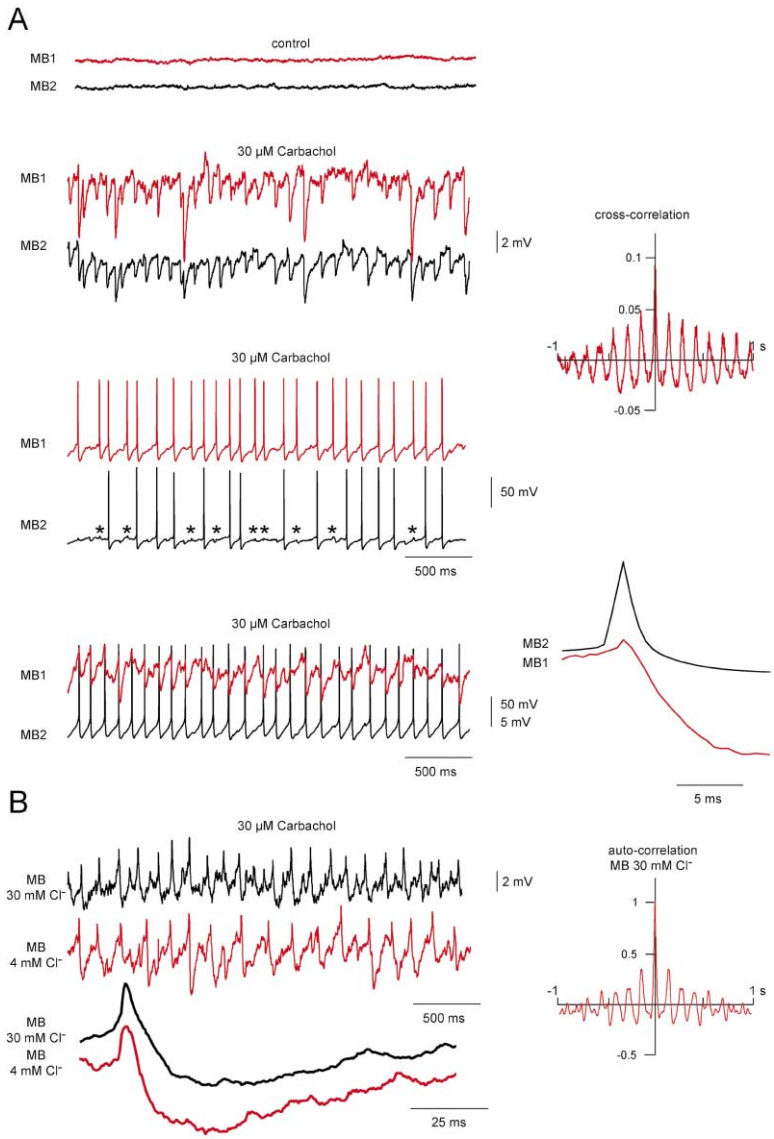

Figure 5. Carbachol-Induced Synchronous Rhythmic Activity in MB Cells

(A) Spontaneous activity in two electrically coupled MB cells prior to carbachol application (upper pair of traces). 30 μM carbachol induces subthreshold (middle pair of traces) or suprathreshold (lower two pairs of traces) theta frequency rhythmic activity in MB cells, which is highly synchronized, as shown by the crosscorrelation on the right (n = 11, pooled data from either sub- or suprathreshold rhythmic activity). No delay can be measured between the AP peak in one MB cell and the onset of the IPSP in the other cell, as shown by the average spike analysis (right panel).

(B) Carbachol-induced oscillation recorded from a MB cell with 30 mM internal chloride concentration. Under these conditions, IPSPs are depolarizing at resting membrane potential (−49 mV). Hyperpolarizing events are most likely gap junction transmitted reflections of APs. The corresponding autocorrelation is shown on the right. The expanded trace at the bottom shows an average of 9 hyperpolarizing events. For comparison, a trace from a recording with normal internal chloride concentration (4 mM, red trace) is added.

reliably reflect phasic inputs, which generate membrane potential fluctuations below 15 Hz (e.g., the electroencephalogram [EEG] theta band) but not inputs that generate higher frequency fluctuations in membrane potential (e.g., the EEG β and γ bands).

Rhythmic activity in hippocampal or cortical slices can be evoked by the application of various substances, such as cholinergic and glutamatergic agonists or potassium channel blockers (Buhl et al., 1998; Buzsaki and Chrobak, 1995; Fisahn et al., 1998; Traub et al., 2000). Recently it has been shown that low threshold spiking (LTS) cells can generate rhythmic activity in the low-frequency band upon the application of ACPD (metabotropic GluR agonist, 50–100 μM; Beierlein et al., 2000), but no effect was observed in MB cells (n = 5, data not shown). However, bath application of the cholinergic agonist carbachol (20–30 μM) caused depolarization (by 13.3 ± 5.7 mV) of MB cells and provoked both spiking and subthreshold membrane potential oscillations in the theta frequency band (5.2 ± 1.17 Hz, Figures 5–8). An individual MB cell would exhibit either exclusively subthreshold or both sub- and suprathreshold rhythmic activity. Out of 125 MB cells tested, all showed clear carbachol-induced membrane potential oscillations within the theta frequency range. Of these 125 cells, 43 demonstrated theta frequency outputs, with the timing of single APs tightly correlated with the peak depolarization of the underlying membrane potential oscillation (Figure 5A). Carbachol-induced oscillations were most likely due to the activation of muscarinic receptors, since they could be blocked by atropine (5 μM, n = 5; Figure 6A) and mimicked by muscarine (100 μM, n = 5, Figure 6B). The amplitude of the oscillatory events and the duration of rhythmic episodes varied from cell to cell. This variability was not dependent on the distance between two MB cells (up to 200 μm). Figure 5A (upper pair of traces) shows example traces of spontaneous activity in two electrically coupled MB cells. Application of 30 μM carbachol induced in all cell pairs (43/43) periods of supra- and/or subthreshold membrane potential oscillations.

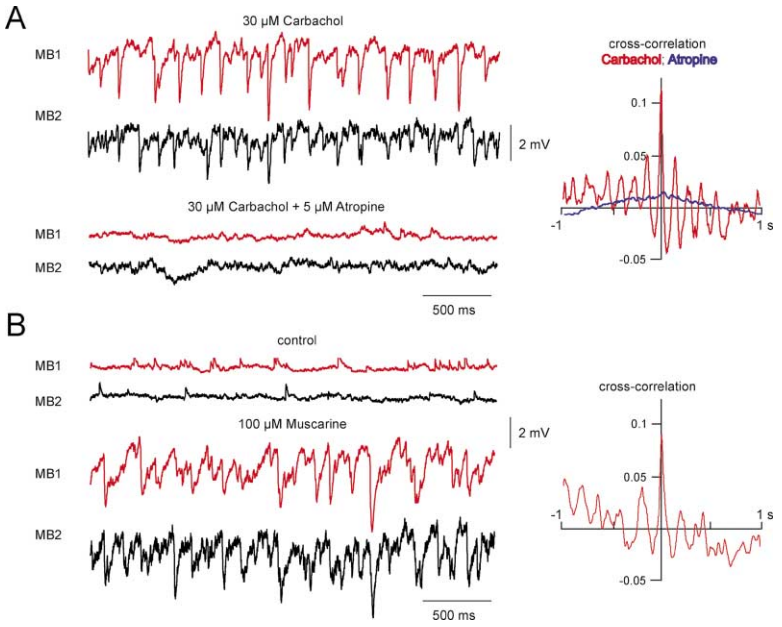

Figure 6. Carbachol-Induced Oscillations Are Most Likely Mediated by Muscarinic Receptors

(A) Atropine blocks carbachol-induced oscillations. 30 μM carbachol induces rhythmic and synchronized activity in two MB cells (upper pair of traces), which was blocked completely by application of 5 μM atropine (lower pair of traces). Corresponding crosscorrelations are shown on the right, in red for carbachol alone and in blue after atropine application (n = 5).

(B) Muscarine can mimic carbachol-induced oscillations. Spontaneous activity in two electrically coupled MB cells prior to muscarine application (upper pair of traces). 100 μM muscarine induces subthreshold theta frequency rhythmic activity in both cells (lower pair of traces), which is highly synchronized, as shown by the crosscorrelation on the right (n = 5).

Subthreshold oscillations were highly synchronized (second pair of traces). Suprathreshold activity was defined by periods of AP generation in one or both cells (lower two pairs of traces). In paired recordings where one MB cell was active and the other quiescent, coincident membrane potential oscillations were still seen. No measurable delay (resolution 0.5 ms) was seen between AP generation in one MB cell and the onset of the IPSP in the other cell. During periods where AP failures occurred in one MB cell, small, brief biphasic membrane potential fluctuations (Figure 5, asterisks) occurred, reminiscent of those generated by depolarization-induced APs in one of a pair of electrically coupled MB cells (see Figure 4A). Reduction of the chloride gradient in single MB cells revealed these putative electrical coupling potentials more clearly (Figure 5B). Such a relationship between threshold and subthreshold activity is typical of networks of mutually interconnected interneurons (see Discussion).

Carbachol-induced oscillations were not dependent on excitatory glutamatergic transmission since the application of NBQX did not have a significant effect on either frequency (control 5.8 ± 0.5 Hz versus NBQX 6.0 ± 0.4 Hz), rhythmicity (height of correlogram side peaks in control 0.03 ± 0.007 versus NBQX 0.030 ± 0.010), or synchrony (height of correlogram central peaks in control 0.052 ± 0.008 versus NBQX 0.046 ± 0.006; Figure 7A, n = 5 for each measurement, $p > 0.05$). Computer modeling and experiments suggest that the interplay between electrical and chemical inhibitory synapses can be crucial for maintaining synchrony of rhythmic activity in the hippocampus and neocortex (Skinner et al., 1999; Tamas et al., 2000; Traub et al., 1999, 2001). On the other hand, rhythmic activity in the LTS cell network did not depend on GABAergic transmission (Beierlein et al., 2000). In the case of the MB cell network, application of the highly selective $GABA_A$ channel blocker SR-95531 (Gabazine, 10 μM) substantially reduced the amplitude of oscillatory events (from 4.83 ± 1.52 to 1.21 ± 0.71 mV) and led to significant reduction in synchrony (measured as height of central peak of the crosscorrelogram: control 0.051 ± 0.005, Gabazine 0.02 ± 0.006, $p < 0.05$, n = 5; Figure 7B). The same effect was observed with the $GABA_A$ channel blocker bicuculline (10 μM, n = 5; data not shown). To test the contribution of electrical coupling to carbachol-induced oscillations in the MB cell network, we analyzed rhythmicity and synchrony in Cx36 knockout mice. Cx36 is the main neuronal connexin (Condorelli et al., 2000) and mediates gap junction coupling between different types of neocortical and hippocampal interneurons (Deans et al., 2001; Venance et al., 2000; Hormuzdi et al., 2001). Electrical coupling was abolished between MB cells in Cx36 knockout mice (n = 25 pairs from 10 animals), whereas chemical transmission between MB cells was comparable to that in wild-type mice (average IPSP1 amplitude 1.16 ± 0.97 mV, average PPR 1.12 ± 0.28, $p > 0.05$, n = 16 pairs from 6 animals, data not shown). Although carbachol could induce some rhythmic activity in MB cells in Cx36 knockout mice, these events were substantially reduced in amplitude compared to wild-type mice (4.84 ± 1.69 mV in wild-type, 1.52 ± 0.6 mV in Cx36 knockout, n = 5 for each measurement). Autocorrelation analysis revealed a significant reduction in rhythmicity of this activity in individual MB cells ($p < 0.05$, from amplitude of autocorrelogram side peaks) and MB cell-MB cell synchrony was abolished (Figure 7C, n = 7, 3 animals). The activity in MB cells in slices from Cx36 knockout mice could not be further altered by the application of bicuculline (n = 4, data not shown). Thus, synchrony in the MB cell network depends on both GABAergic chemical transmission and electrical coupling (see Discussion).

Simultaneous recordings from MB cells and FS cells showed that in contrast to MB cells, FS cells were almost not depolarized in the presence of either carbachol (n = 10) or muscarine (n = 3) and demonstrated only weak rhythmic activity upon carbachol application. Crosscor-

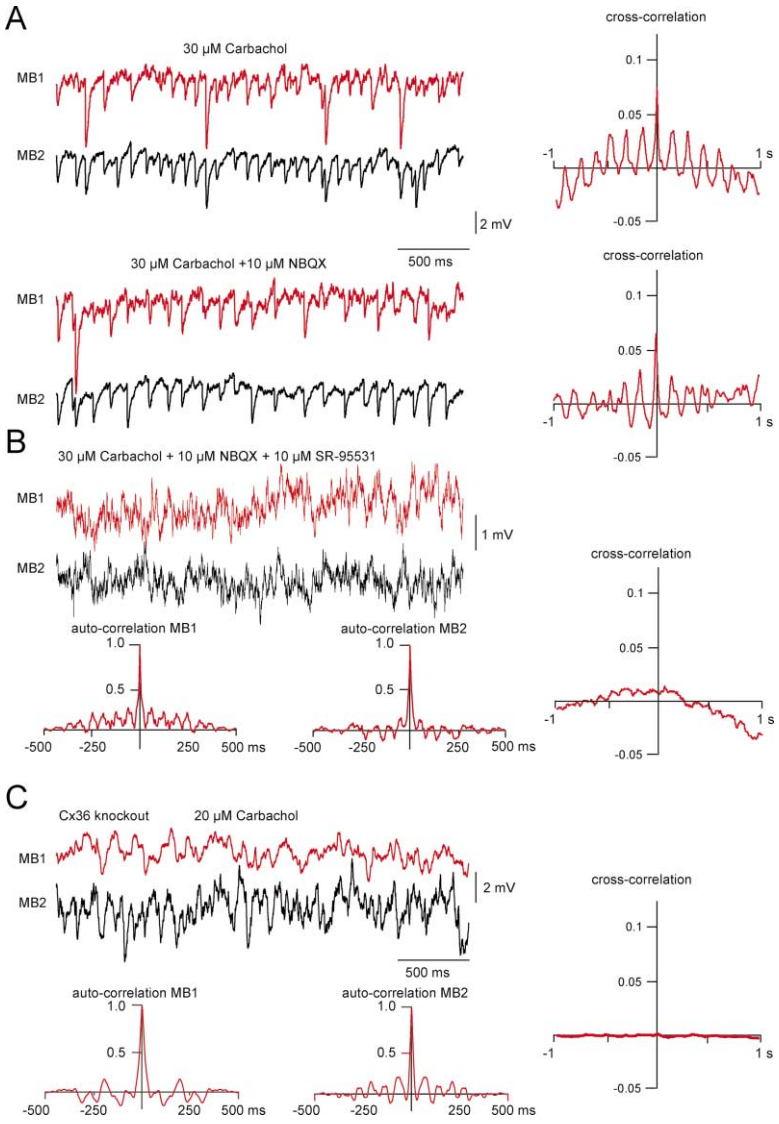

Figure 7. Synchrony Requires both GABAergic Synaptic Transmission and Electrical Coupling

(A) Carbachol-induced oscillations are not sensitive to NBQX (n = 5).

(B) Synchrony of carbachol-induced oscillations is disrupted by 10 μM of the selective $GABA_A$ channel blocker SR-95531, as shown by the crosscorrelation on the right, whereas some rhythmic activity in individual cells persists (autocorrelations for each cell are shown below the traces). Recordings in (A) and (B) were obtained from the same pair.

(C) Synchrony of carbachol-induced oscillations is abolished in slices from Cx36 knockout mice as shown by the crosscorrelation on the right (n = 7, pooled data). However, carbachol can still induce some rhythmic activity in individual MB cells (autocorrelations for each cell are shown below the traces).

relograms of MB cell and FS cell activity demonstrated no synchrony between the activities of these two cell types (Figure 8A). However, when the FS cell was depolarized artificially to the same potential as the MB cell was depolarized by carbachol, we observed IPSPs in the FS cell which were synchronized with the oscillatory events in the MB cell (height of crosscorrelogram at 0 ms was 0.06 ± 0.01; Figure 8A, n = 5). However, rhythmicity was poor in comparison to paired MB cell recordings (compare height of correlogram side peaks in Figure 8A with Figure 5A).

To confirm our hypothesis that a network of MB cells can provide synchronous inhibition of downstream principal neurons, we recorded simultaneously from MB cells and pyramidal cells in the presence of carbachol. In 14 out of 21 pairs, subthreshold oscillations in MB cells were correlated with IPSPs recorded from pyramidal cells, independent of whether the cells were synaptically connected or not (Figure 8B). In these experiments, carbachol did not affect the resting membrane potential of the pyramidal cells. Analysis of suprathreshold oscillations in MB cells and pyramidal cell pairs showed a mean delay of 1.0 ± 0.5 ms from the peak of the MB cell AP to the onset of the pyramidal neuronal IPSP (Figure 8C, n = 5 AP/IPSP pairs per n = 7 MB cell/pyramidal cell pairs). This is in contrast to the simultaneous peaking of MB cell APs and MB cell IPSPs illustrated in Figure 5A.

Discussion

Synchronous activity of neuronal ensembles is thought to be a key element underlying a wide range of information processing in the brain (Singer and Gray, 1995). GABAergic interneurons form distinct networks that can effectively synchronize and coordinate the activity of their target cells via chemical and electrical coupling (Beierlein et al., 2000; Galarreta and Hestrin, 1999; Gibson et al., 1999; Szabadics et al., 2001; Tamas et al., 2000; Venance et al., 2000).

In this study we describe a new interneuron subtype, which is PV positive, yet differs in many respects from

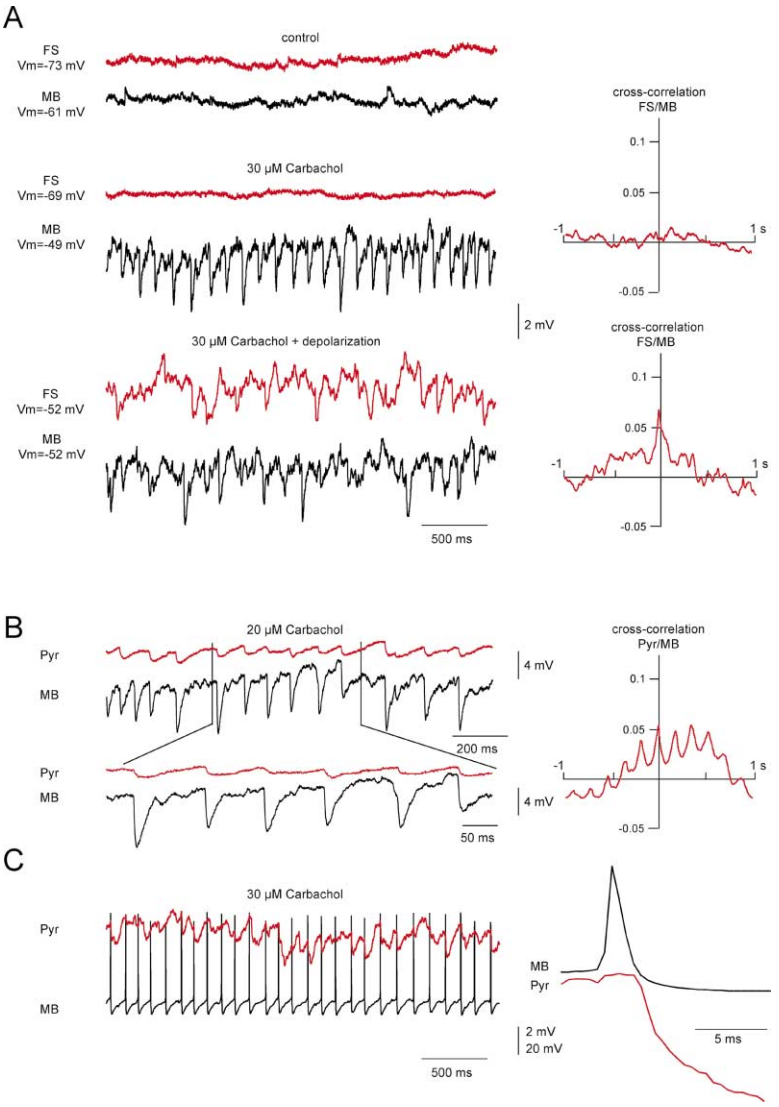

Figure 8. The MB Cell Network Can Phase the Activity of Principal Cells

(A) Carbachol-induced oscillations in MB cells are coherent with FS cell activity, when the FS cell is depolarized artificially.

(B) Carbachol-induced activity in the MB cell network was projected onto pyramidal cells (as IPSP trains).

(C) Carbachol-induced spiking in MB cells triggers IPSPs in pyramidal cells. For these experiments, those pairs were selected that were not directly synaptically connected. The spike average analysis on the right shows mean temporal relationship between action potential spiking in a MB cell and the onset of the IPSP in a concurrently recorded pyramidal cell (n = 5 periods).

the majority of PV-positive cells, the FS cells. MB cells and FS cells respond with a different spiking pattern upon current injection. Both cell types are PV positive but MB cells additionally express CB. The more localized axonal arborization of FS cells contrasts with the broader axonal projection area of MB cells. FS cells have been shown to be basket or axo-axonic cells (Kawaguchi and Kubota, 1997), whereas MB cells are dendritic inhibitory cells. FS cells (Reyes et al., 1998) and MB cells form reciprocal synapses with neighboring pyramidal cells. Interestingly, synaptic connectivity between MB cells and FS cells is unidirectional, with MB cells innervating FS cells but not vice versa. Most importantly, inhibitory synapses established by FS cells and MB cells differ in their short-term synaptic plasticity. Synapses formed by FS cells onto FS cells or pyramidal cells show paired-pulse depression (Reyes et al., 1998), in contrast to MB cell to MB cell and MB cell to pyramidal cell synapses, which exhibit pronounced PPF. Both FS cells and MB cells are coupled with cells of the same type via gap junctions. In addition to electrical coupling, GABAergic neurotransmission appears to be an important requirement in FS cell and MB cell networks for the generation of rhythmic activity albeit in a different frequency range. FS cells, which are thought to participate in γ frequency oscillations (Sik et al., 1997; Tamas et al., 2000), did not show rhythmic activity upon carbachol application alone. In MB cells, on the other hand, carbachol induces rhythmic and synchronous activity within the theta frequency band (5.2 $\pm$ 1.17 Hz).

A recent report by Connors and colleagues describes the LTS cell network in layer 4 of the neocortex that can generate low-frequency rhythmic activity (Beierlein et al., 2000). Even though the LTS cell and MB cell network share the feature of generating low-frequency oscillations, the two networks differ in a number of characteristics. First, LTS cells and MB cells differ in their firing patterns and the expression of neurochemical markers (Gibson et al., 1999). Second, synaptic connections between LTS and FS cells are reciprocal, whereas MB cells innervate FS cells, but not vice versa. Third, ACPD, which can induce low-frequency rhythmic activity in LTS cells, fails to provoke these effects in MB cells, which, however, exhibit rhythmic activity upon carbachol appli-

cation. Finally, synchrony in the LTS cell network requires electrical synapses but not chemical neurotransmission in contrast to the MB cell network where synchrony depends on electrical coupling and GABAergic synaptic transmission. Moreover, when either GABAergic transmission or electrical coupling between MB cells was disrupted, the mean amplitude of oscillatory events was reduced to the same extent.

Of note is that NBQX did not significantly affect carbachol-induced oscillations in the MB cell network, indicating that MB cells can generate and maintain synchronous theta frequency rhythmic activity without the need of phasic excitatory glutamatergic input. Taken together, the data suggest that MB cells form a novel interneuron network, which can induce synchronized IPSPs in populations of layer 2/3 pyramidal cells and thereby phase their firing activity. The form of this activity appeared to be a genuine network phenomenon: not all MB cells tested generated theta frequency outputs at any one time, but APs generated in active MB cells occurred simultaneously with the peak depolarizing part of the corresponding subthreshold oscillation in inactive MB cells. Both IPSP trains and APs (when present in MB cell pairs) occurred synchronously. Rhythmic subthreshold membrane potential activity contained components from at least three sources: IPSPs from other MB cells within the network; direct membrane potential deviations from electrical coupling to other MB cells; and intrinsic oscillatory membrane potential changes in response to cholinergic depolarization. Thus, removing either the electrical coupling *or* the mutual phasic inhibition did not completely abolish rhythmic activity in individual MB cells, but did remove MB cell-MB cell synchrony. Synchrony between the oscillatory activity in MB cells and IPSPs in pyramidal cells, even when the two cells were not directly coupled, further suggested that it was the net, synchronous output from the MB cell network that provided the phasic inhibitory cues to pyramidal cells. Our data is entirely consistent with a MB cell network being the source of the rhythm. We cannot, unequivocally, rule out the involvement of other cell types. However, any cell acting as a source for this rhythm would have to be (1) inhibitory, (2) mutually synaptically connected to MB cells, and (3) electrically connected to MB cells to explain the data we have. It is not impossible that there are cells in the cortex that are excited by carbachol and meet points (1) and (2). However, to date the vast majority of electrical connectivity in the cortex has been seen only between homogeneous cell types and not between different cell types.

In the presence of cholinergic drive alone, little synchrony is seen between the activities of MB cells and FS cells. However, we demonstrated that there was an inhibitory synaptic connection between MB cells and FS cells. Since neither carbachol nor muscarine directly depolarized FS cells, the possibility that MB cells can also modulate FS cell output cannot be ruled out. Direct depolarization of FS cells via the recording electrode revealed trains of IPSPs that were weakly temporally correlated with carbachol-induced MB cell activity, suggesting that MB cell inputs to FS cells form only a small proportion of this cell type's synaptic inhibitory input. FS cells have been shown to be involved in generating γ frequency oscillations, and Buhl et al. (1998) showed that coapplication of kainate and carbachol was required to generate this rhythm in the neocortex.

Since the excitatory input to MB cells from layer 2/3 pyramidal cells is relatively rare and mean amplitudes of first EPSPs are relatively small, MB cells most likely receive excitation from other brain regions and/or neocortical layers. In experiments in which we recorded EPSPs from MB cells evoked by extracellular stimulation in layers 2/3, 4, and 5, respectively, the largest response was obtained when the stimulation pipette was placed in layer 4. Responses to stimulation either in layers 2/3 or 5 were significantly smaller (unpublished observation). This implies that MB cells either receive direct thalamic excitatory drive or are innervated by layer 4 spiny stellate cells, which target mainly layer 2/3 and 4 excitatory cells (Lubke et al., 2000) and are considered to be the first element involved in intracortical signaling processing (McCormick, 1992). One could speculate that in the hierarchy of cortical information processing, MB cells form an inhibitory network that controls cortical inputs by coordinating the activity of layer 2/3 pyramidal cells.

Experimental Procedures

Electrophysiology

Transverse neocortical slices of 250 μm thickness were prepared from the brains of 14-day-old PV-EGFP (Meyer et al., 2002), Cx36 knockout (Hormuzdi et al., 2001), and C57Bl6 mice. Brain slice preparation and visualization of neurons both in living slices and after labeling with biocytin are described elsewhere (Markram et al., 1997; Stuart et al., 1993). During recordings, slices were maintained at room temperature (22°C–24°C) in extracellular solution consisting of (in mM): 125 NaCl, 2.5 KCl, 25 glucose, 25 $NaHCO_3$, 1.25 NaH_2PO_4, 2 $CaCl_2$, and 1 $MgCl_2$ (pH 7.2 when bubbled with carbogen). Whole-cell voltage recordings were performed simultaneously from two neurons using pipettes with resistance of 5–7 MOhm when filled with (in mM): 105 K gluconate, 30 KCl, 4 Mg-ATP, 10 phosphocreatine, 0.3 GTP, and 10 HEPES (pH 7.3, KOH, 293 mOsm). In synaptically connected neurons, suprathreshold intracellular stimulation of presynaptic cells evoked depolarizing EPSPs or IPSPs recorded from postsynaptic cells. Presynaptic cells were stimulated with a 10 Hz train of 3 suprathreshold current pulses. Trains were delivered at intervals of 7 s. Voltage traces shown are averages of 50–100 sweeps. Electrically coupled cells were 40 to 200 μm apart. After establishing the whole-cell mode, depolarizing and hyperpolarizing current pulses were applied to one of the potentially coupled neurons. Voltage responses recorded in current clamp mode from the other cell indicated electrical coupling between these neurons. The coupling coefficient between two cells was determined as the ratio of the voltage response in cell 2 divided by the voltage response in cell 1 under steady-state conditions. The success rate of finding an electrical or chemical coupling was calculated as the inverse (in %) of the number of neurons tested before a connection was found. To estimate the amplitude of the second IPSP, the decay of the first IPSP was fitted with a double exponential and extrapolated to the time corresponding to the peak of the IPSP. The IPSP amplitude was defined as the difference between the IPSP peak and the value of the extrapolated fit at the time of the peak. Stimulus delivery and data acquisition was performed using PULSE software (HEKA Elektronik, Lambrecht, Germany). Analyses were performed using IGOR PRO software (Wavemetrics, Lake Oswego, OR).

In oscillation experiments, recordings were done at 32°C and except for the high-chloride experiments described in Figure 5B, low chloride-containing intracellular solution was used. This solution contained (in mM): 130 K gluconate, 10 Na gluconate, 4 NaCl, 4 Mg-ATP, 10 phosphocreatine, 0.3 GTP, and 10 HEPES (pH 7.3, KOH, 305 mOsm). The following drugs were used: (1S,3R)-1-aminocyclopentane-1,3-dicarboxylic acid ((1S,3R)-ACPD, Tocris, Bristol, UK), muscarine chloride (ICN Biomedicals Inc., Eschwege, Germany), carbachol, SR95531 (Gabazine), and atropine (Sigma, Steinheim,

Germany). Temporal patterns of observed oscillatory activity were quantified using standard two-dimensional correlation analysis (Matlab, Mathworks, Natick, MA). Synchrony was quantified as the height of the central peak of correlograms at the intercept with the *y* axis. Data in the graphs and text are given as the mean ± SD. Calculation of the statistical significance of differences was performed using unpaired, two-tailed Student's t test.

Morphological Reconstruction

For morphological reconstruction, cells were filled with biocytin (2%) added to the intracellular pipette solution. Slices were fixed with 2% paraformaldehyde overnight and cryoprotected with 30% sucrose; then they were permeabilized by freezing over liquid nitrogen, quenched in 1% H_2O_2, and incubated with avidin-biotin-horseradish peroxidase complex (Elite ABC, Vector Laboratories, Burlingame, CA). The immunoperoxidase reaction was developed using 3-3′-diaminobenzidine (DAB, Sigma, Steinheim, Germany) intensified with nickel-sulfate (DAB-nickel) as chromogen. After development of the biocytin labeling with DAB-nickel-peroxidase, slices were resliced into 60 μm thick sections. Sections were osmificated and dehydrated in ascending alcohol series and in propylene-oxide and were finally embedded into Durcupan (ACM, Fluka, Buchs, Switzerland). Morphological reconstruction and Sholl analysis of labeled cells after fixation and processing was subsequently made using the Neurolucida tracing program (MicroBrightField, Colchester, VT). For each cell, the dendritic and axonal distribution was analyzed by calculating the total length and the number of interceptions of dendrites or axons with concentric spheres around the cell body (radius increment of 10 μm). Data in Sholl plots are given as the mean ± SEM. Calculation of the statistical significance of differences was performed using unpaired, two-tailed Student's t test.

Immunocytochemistry

For immunocytochemistry, individual cells were filled with biocytin for 1.5–3 min, and slices were postfixed with 4% paraformaldehyde overnight at 4°C. Slices were embedded in 4% agar (Fluka, Buchs, Switzerland), subsliced into 50 μm thick sections on a vibratome (Leica VT1000S, Heidelberg, Germany), and transferred into 50 mM Tris-HCl (pH 7.4), 1.5% NaCl (TBS). For colocalization studies, 50 μm sections were sliced from P14 or P28 mouse brains fixed with 4% paraformaldehyde. Sections were permeabilized in TBS, 0.4% Triton X-100 (Sigma, Steinheim, Germany) for 30 min followed by preincubation in TBS, 4% normal goat serum (NGS), 0.2% Triton X-100 for 30 min and incubation in 2% NGS, 0.1% Triton X-100 at 4°C overnight with polyclonal or monoclonal antibodies against PV (Sigma, 1:1000), CB, CR (Swant, Bellinzona, Switzerland, 1:3000), or VIP (1:500, Incstar, Stillwater, MN). Sections were washed three times for 10 min with cold TBS and incubated for 2.5 hr in fluorescin-isothiocyanate (FITC)- or Texas red-conjugated secondary antibodies (1:400). The biocytin-filled cells were visualized by FITC-conjugated avidin (3 μg/ml, Jackson Immuno Research, West Grove, PA). Sections were washed twice for 10 min in TBS, 1% NGS and twice in TBS. After a brief rinse in bidistilled H_2O, sections were air-dried and mounted in Mowiol (Polysciences, Warrington, UK). Immunostained sections were visualized under epifluorescent illumination with a BX51 microscope (Olympus, Japan).

Electronmicroscopy

After development of the biocytin labeling, slices were resliced into 60 μm thick sections. Sections were osmificated and dehydrated in ascending alcohol series and in propylene-oxide and were finally embedded into Durcupan (ACM, Fluka, Buchs, Switzerland). Regions containing the highest density of axon terminals in layer 2/3 were selected and photographed in the light microscope and then reembedded into Durcupan blocks. Then, 60 nm thick serial sections were cut with a Reichert ultramicrotome, placed onto copper grids coated with Formwar (SERVA, Heidelberg, Germany), and analyzed in a Zeiss electron microscope (Jena, Germany). Biocytin-filled axon terminals were then identified randomly and followed through several serial sections until the nature of the synaptic connections and postsynaptic targets were clearly established.

Acknowledgments

We thank Drs. P.H. Seeburg, E. Fuchs, T. Freund, N. Urban, T. Margrie, N. Burnashev, and R.D. Traub for their comments on the manuscript and useful discussions and A. Helwig and Dr. N. Hajos for help with electronmicroscopy. This work was supported in part by the Schilling Foundation and Novartis. M.B. was supported by the Graduate Program of Molecular and Cellular Neurobiology of the University of Heidelberg. I.K. was a recipient of an EMBO long-term fellowship. M.A.W. was supported by The Wellcome Trust.

Received: June 4, 2002
Revised: March 17, 2003
Accepted: May 9, 2003
Published: June 4, 2003

References

Alcantara, S., de Lecea, L., Del Rio, J.A., Ferrer, I., and Soriano, E. (1996). Transient colocalization of parvalbumin and calbindin D28k in the postnatal cerebral cortex: evidence for a phenotypic shift in developing nonpyramidal neurons. Eur. J. Neurosci. *8*, 1329–1339.

Beierlein, M., Gibson, J.R., and Connors, B.W. (2000). A network of electrically coupled interneurons drives synchronized inhibition in neocortex. Nat. Neurosci. *3*, 904–910.

Buhl, E.H., Tamas, G., and Fisahn, A. (1998). Cholinergic activation and tonic excitation induce persistent gamma oscillations in mouse somatosensory cortex in vitro. J. Physiol. *513*, 117–126.

Buzsaki, G., and Chrobak, J.J. (1995). Temporal structure in spatially organized neuronal ensembles: a role for interneuronal networks. Curr. Opin. Neurobiol. *5*, 504–510.

Caputi, A., Meyer, A., Fuchs, E., and Monyer, H. (2000). Generation of transgenic mice expressing a green fluorescent protein in calretinin-positive neurons. Paper presented at: Society for Neuroscience Meeting (New Orleans, LA).

Cauli, B., Porter, J.T., Tsuzuki, K., Lambolez, B., Rossier, J., Quenet, B., and Audinat, E. (2000). Classification of fusiform neocortical interneurons based on unsupervised clustering. Proc. Natl. Acad. Sci. USA *97*, 6144–6149.

Cobb, S.R., Buhl, E.H., Halasy, K., Paulsen, O., and Somogyi, P. (1995). Synchronization of neuronal activity in hippocampus by individual GABAergic interneurons. Nature *378*, 75–78.

Condorelli, D.F., Belluardo, N., Trovato-Salinaro, A., and Mudo, G. (2000). Expression of Cx36 in mammalian neurons. Brain Res. Brain Res. Rev. *32*, 72–85.

Deans, M.R., Gibson, J.R., Sellitto, C., Connors, B.W., and Paul, D.L. (2001). Synchronous activity of inhibitory networks in neocortex requires electrical synapses containing connexin36. Neuron *31*, 477–485.

Du, J., Zhang, L., Weiser, M., Rudy, B., and McBain, C.J. (1996). Developmental expression and functional characterization of the potassium-channel subunit Kv3.1b in parvalbumin-containing interneurons of the rat hippocampus. J. Neurosci. *16*, 506–518.

Fisahn, A., Pike, F.G., Buhl, E.H., and Paulsen, O. (1998). Cholinergic induction of network oscillations at 40 Hz in the hippocampus in vitro. Nature *394*, 186–189.

Freund, T.F., and Buzsaki, G. (1996). Interneurons of the hippocampus. Hippocampus *6*, 347–470.

Galarreta, M., and Hestrin, S. (1999). A network of fast-spiking cells in the neocortex connected by electrical synapses. Nature *402*, 72–75.

Geiger, J.R., Lubke, J., Roth, A., Frotscher, M., and Jonas, P. (1997). Submillisecond AMPA receptor-mediated signaling at a principal neuron-interneuron synapse. Neuron *18*, 1009–1023.

Gibson, J.R., Beierlein, M., and Connors, B.W. (1999). Two networks of electrically coupled inhibitory neurons in neocortex. Nature *402*, 75–79.

Gupta, A., Wang, Y., and Markram, H. (2000). Organizing principles for a diversity of GABAergic interneurons and synapses in the neocortex. Science *287*, 273–278.

Hormuzdi, S.G., Pais, I., LeBeau, F.E., Towers, S.K., Rozov, A., Buhl,

E.H., Whittington, M.A., and Monyer, H. (2001). Impaired electrical signaling disrupts gamma frequency oscillations in connexin 36-deficient mice. Neuron *31*, 487–495.

Kawaguchi, Y. (1995). Physiological subgroups of nonpyramidal cells with specific morphological characteristics in layer II/III of rat frontal cortex. J. Neurosci. *15*, 2638–2655.

Kawaguchi, Y., and Kubota, Y. (1997). GABAergic cell subtypes and their synaptic connections in rat frontal cortex. Cereb. Cortex *7*, 476–486.

Lubke, J., Egger, V., Sakmann, B., and Feldmeyer, D. (2000). Columnar organization of dendrites and axons of single and synaptically coupled excitatory spiny neurons in layer 4 of the rat barrel cortex. J. Neurosci. *20*, 5300–5311.

Markram, H., Lubke, J., Frotscher, M., Roth, A., and Sakmann, B. (1997). Physiology and anatomy of synaptic connections between thick tufted pyramidal neurones in the developing rat neocortex. J. Physiol. *500*, 409–440.

Martina, M., Schultz, J.H., Ehmke, H., Monyer, H., and Jonas, P. (1998). Functional and molecular differences between voltage-gated K+ channels of fast-spiking interneurons and pyramidal neurons of rat hippocampus. J. Neurosci. *18*, 8111–8125.

McBain, C.J., and Fisahn, A. (2001). Interneurons unbound. Nat. Rev. Neurosci. *2*, 11–23.

McCormick, D.A. (1992). Neurotransmitter actions in the thalamus and cerebral cortex and their role in neuromodulation of thalamocortical activity. Prog. Neurobiol. *39*, 337–388.

Meyer, A.H., Katona, I., Blatow, M., Rozov, A., and Monyer, H. (2002). In vivo labeling of parvalbumin-positive interneurons and analysis of electrical coupling in identified neurons. J. Neurosci. *22*, 7055–7064.

Penttonen, M., Kamondi, A., Acsady, L., and Buzsaki, G. (1998). Gamma frequency oscillation in the hippocampus of the rat: intracellular analysis in vivo. Eur. J. Neurosci. *10*, 718–728.

Reyes, A., Lujan, R., Rozov, A., Burnashev, N., Somogyi, P., and Sakmann, B. (1998). Target-cell-specific facilitation and depression in neocortical circuits. Nat. Neurosci. *1*, 279–285.

Rozov, A., Jerecic, J., Sakmann, B., and Burnashev, N. (2001). AMPA receptor channels with long-lasting desensitization in bipolar interneurons contribute to synaptic depression in a novel feedback circuit in layer 2/3 of rat neocortex. J. Neurosci. *21*, 8062–8071.

Sik, A., Penttonen, M., and Buzsaki, G. (1997). Interneurons in the hippocampal dentate gyrus: an in vivo intracellular study. Eur. J. Neurosci. *9*, 573–588.

Singer, W., and Gray, C.M. (1995). Visual feature integration and the temporal correlation hypothesis. Annu. Rev. Neurosci. *18*, 555–586.

Skinner, F.K., Zhang, L., Velazquez, J.L., and Carlen, P.L. (1999). Bursting in inhibitory interneuronal networks: a role for gap- junctional coupling. J. Neurophysiol. *81*, 1274–1283.

Somogyi, P., Tamas, G., Lujan, R., and Buhl, E.H. (1998). Salient features of synaptic organisation in the cerebral cortex. Brain Res. Brain Res. Rev. *26*, 113–135.

Stuart, G.J., Dodt, H.U., and Sakmann, B. (1993). Patch-clamp recordings from the soma and dendrites of neurons in brain slices using infrared video microscopy. Pflugers Arch. *423*, 511–518.

Szabadics, J., Lorincz, A., and Tamas, G. (2001). Beta and gamma frequency synchronization by dendritic gabaergic synapses and gap junctions in a network of cortical interneurons. J. Neurosci. *21*, 5824–5831.

Tamas, G., Buhl, E.H., Lorincz, A., and Somogyi, P. (2000). Proximally targeted GABAergic synapses and gap junctions synchronize cortical interneurons. Nat. Neurosci. *3*, 366–371.

Traub, R.D., Bibbig, A., Fisahn, A., LeBeau, F.E., Whittington, M.A., and Buhl, E.H. (2000). A model of gamma-frequency network oscillations induced in the rat CA3 region by carbachol in vitro. Eur. J. Neurosci. *12*, 4093–4106.

Traub, R.D., Jefferys, J.G.R., and Whittington, M.A. (1999). Fast Oscillation in Cortical Circuits (Cambridge, MA: MIT Press).

Traub, R.D., Kopell, N., Bibbig, A., Buhl, E.H., LeBeau, F.E., and Whittington, M.A. (2001). Gap junctions between interneuron dendrites can enhance synchrony of gamma oscillations in distributed networks. J. Neurosci. *21*, 9478–9486.

Tsodyks, M., Uziel, A., and Markram, H. (2000). Synchrony generation in recurrent networks with frequency-dependent synapses. J. Neurosci. *20*, RC50.

van Brederode, J.F., Helliesen, M.K., and Hendrickson, A.E. (1991). Distribution of the calcium-binding proteins parvalbumin and calbindin-D28k in the sensorimotor cortex of the rat. Neuroscience *44*, 157–171.

Venance, L., Rozov, A., Blatow, M., Burnashev, N., Feldmeyer, D., and Monyer, H. (2000). Connexin expression in electrically coupled postnatal rat brain neurons. Proc. Natl. Acad. Sci. USA *97*, 10260–10265.

Whittington, M.A., Traub, R.D., and Jefferys, J.G. (1995). Synchronized oscillations in interneuron networks driven by metabotropic glutamate receptor activation. Nature *373*, 612–615.

Ylinen, A., Bragin, A., Nadasdy, Z., Jando, G., Szabo, I., Sik, A., and Buzsaki, G. (1995a). Sharp wave-associated high-frequency oscillation (200 Hz) in the intact hippocampus: network and intracellular mechanisms. J. Neurosci. *15*, 30–46.

Ylinen, A., Soltesz, I., Bragin, A., Penttonen, M., Sik, A., and Buzsaki, G. (1995b). Intracellular correlates of hippocampal theta rhythm in identified pyramidal cells, granule cells, and basket cells. Hippocampus *5*, 78–90.